JOURNAL OF SOLID STATE CHEMISTRY **132,** 98–106 (1997)
ARTICLE NO. SC977414

Structure and Properties of the $Pr_{1-x}K_xMnO_3$ Perovskites ($x = 0$–0.15)

Z. Jirák[1], J. Hejtmánek, and K. Knížek

Institute of Physics, Cukrovarnická 10, 162 00 Prague 6, Czech Republic

and

R. Sonntag

Hahn-Meitner-Institut, Glienicker Strasse 100, 1000 Berlin 39, Germany

Received July 8, 1996; in revised form January 15, 1997; accepted April 7, 1997

The mixed-valence manganites $Pr_{1-x}K_xMnO_3$ have been prepared up to maximum content of 30% Mn^{4+} ($x = 0.15$ in the ideal case) and investigated by the neutron diffraction and electric transport measurements. Similar to related systems with divalent alkali earths, the increasing monovalent potassium substitution generates mobile charge carriers and changes gradually the magnetic ordering from the layered antiferromagnetism through canted arrangements to a pure ferromagnetism. The ferromagnetic transition for sample with $x \geq 0.10$ is associated with an anomaly in the temperature dependences of the resistivity, thermopower, and a local maximum of the magnetoresistance. The insulator–metal transition is absent up to 30% Mn^{4+} despite the expectations based on the mean large cation size. An unexpected increase of the negative magnetoresistance is observed $x = 0.15$ at low temperatures where the magnetization is already saturated.

INTRODUCTION

Present interest in perovskites with Mn^{3+}/Mn^{4+} ions is stimulated by the observation of electronic transitions which are related to the structural and magnetic ordering phenomena. The most studied systems are the lanthanum-based manganites $La^{3+}_{1-x}A^{2+}_xMn^{3+}_{1-x}Mn^{4+}_xO_3$ (A = Ca, Sr, Ba, or Pb) which for $0.17 \leq x \leq 0.4$ become ferromagnets and exhibit an insulator–metal (I–M) transition close to the Curie temperature. Moreover, in a broad temperature region a considerable decrease of the resistivity in magnetic field is observed and this effect can be enhanced enormously using certain technological procedures by introduction of inhomogeneities (See, e.g., Refs. 1–3). Similar behavior to that for the lanthanum-based perovskites is encountered also for their rare-earth homologues. As to the praseodymium systems, systematic investigations of the crystal and magnetic structures on samples with defined Mn^{4+} content have been performed previously for the Ca^{2+}, Sr^{2+}, and Ba^{2+} substitutions (4–6).

The $Pr_{1-x}Ca_xMnO_3$ series exists in the whole range of $0 \leq x \leq 1$ (4). Solid solutions exhibit a superstructure $\sqrt{2}a_p \times \sqrt{2}a_p \times 2a_p$ with respect to the cubic perovskite and possess an orthorhombic symmetry *Pbnm* above the room temperature. Below room temperature the system exhibits very rich structural and magnetic phase diagram which can be related to different kinds of manganese valence distribution and d_γ orbital ordering of Mn^{3+} ions (the Jahn–Teller effect). Ferromagnetism is restricted to a narrow range of $x \sim 0.2$–0.3 and the samples remain semiconducting below the Curie temperature ($T_C \sim 120$–130 K). The metallic state can be induced, however, for $x = 0.3$ by applying the external magnetic field during the sample cooling (7) or by a small substitution of calcium with strontium (8).

The existence of the perovskite phases $Pr_{1-x}Sr_xMnO_3$ and $Pr_{1-x}Ba_xMnO_3$ is limited to about $x = 0.5$ (5) and 0.4 (6), respectively. Pure ferromagnetism appears at $x \sim 0.2$ and the metallic conductivity at low temperatures is observed in both systems for $0.3 \leq x \leq 0.4$. The Curie temperatures for the strontium and barium series culminate at 295 and 195 K, respectively. It should be noted that the $Pr_{1-x}Ba_xMnO_3$ system shows at $x \sim 0.2$ a phase boundary between the common orthorhombic structure of the *Pbnm* symmetry and another one of the *Ibmm* symmetry. Moreover, for $x \sim 0.35$ there is a transition close to the room temperature from the orthorhombic *Ibmm* structure to a tetragonal one of the *I*4/*mcm* symmetry (6). These distinct structures are associated with different arrangements of tilted MnO_6 octahedra and reflect the increasing mean size of large cations in these perovskites.

The above mentioned structural and magnetic diversity of substituted praseodymium perovskites makes a complex

[1]To whom correspondence should be addressed.

0022-4596/97 $25.00

study of further systems actual. The present paper summarizes the experiments on a novel series with the monovalent substitution $Pr^{3+}_{1-x}K^{+}_{x}Mn^{3+}_{1-2x}Mn^{4+}_{2x}O_3$.

EXPERIMENTAL

Ceramic synthesis of $Pr_{1-x}K_xMnO_3$ has been undertaken from the potassium-free composition $x = 0$ in steps of 0.05 up to $x = 0.25$. The mixtures of appropriate amounts of Pr_6O_{11}, K_2CO_3, and $MnCO_3$ were calcined at 850°C, pressed into pellets, and sintered in air under different conditions depending on the potassium content. The sample $x = 0$ was fired at 1260°C with duration of 36 hours and air quenched. The potassium-substituted compounds were sintered at 1200°C for 50–70 hours and subsequently cooled by switching off the furnace. In order to preserve the ideal oxygen stoichiometry, the products were additionally annealed at different temperatures and oxygen pressures as described below. Density of fabricated $Pr_{1-x}K_xMnO_3$ ceramics achieved 92% of the theoretical value for $x = 0$ and decreased gradually with increasing potassium content down to 78% for $x \geq 0.15$.

The X-ray analysis carried out on a diffractometer DRON-3 (Cu$K\alpha$ radiation, Ni filter, $\lambda = 1.54178$ Å) has shown a pure perovskite phase for samples $x \leq 0.15$. Using the Rietveld refinement of observed spectra for sample $x = 0.25$ in which the presence of the Mn_3O_4 impurity was clearly seen the maximum potassium solubility of about $x = 0.175$ in the $Pr_{1-x}K_xMnO_3$ perovskites was estimated. The chemical composition and its spacial homogeneity together with the potassium solubility limit were further checked using the electron microprobe X-ray analyzer JEOL JXA 733. Moreover, these quantities were additionally tested by the refinement of the neutron diffraction data.

The actual Mn^{4+} content and subsequently deduced oxygen stoichiometry were determined by the wet chemical analysis based on the reduction of $Mn^{3+,4+}$ ions by Fe^{2+}. The furnace cooled samples revealed generally Mn^{4+} excess ($x = 0.05$) or deficiency ($x = 0.15$) with respect to the chemical composition and ideal stoichiometry. In order to make the samples stoichiometric, the $x = 0.05$ ceramics was reduced by annealing for 1 hour at 1200°C in air and subsequent quenching. On the other hand, the sample with $x = 0.15$ was oxidized for 3 days at 770°C in the oxygen flow. In this respect we note that no bulk intake of oxygen was observed at temperatures below 750°C.

DC resistivity measurements were carried out in the temperature range 4.2–300 K using a classic four-probe method. Small platelets were cut from the sintered pellets and four electrical contacts of about 0.01 mm^2 on the circumference of the sample were made using silver paint and fired at 400°C. Absolute values of the electrical resistivity were evaluated using the Van der Pauw method. For $Pr_{0.85}K_{0.15}MnO_3$, the temperature dependence of resistivity was measured also in a magnetic field of 5 T (on a field-cooled sample).

A dynamic two-point method was employed for measurements of the thermoelectric power. The platelets were attached with silver paint to two small copper blocks. Using two miniheaters a variable temperature gradient up to 1 K was developed between the copper blocks and monitored by Pt resistors. The assembly was placed in a closed-cycle He cryostat and the measurements were carried out while slowly increasing the temperature from 15 to 300 K. The thermoelectric voltage vs temperature gradient was monitored and used for the calculation of the thermopower coefficient.

Magnetoresistance measurements were carried out at selected temperatures above and below the Curie temperature using the AC phase sensitive four-probe technique. The amplitude and frequency of the electrical current applied within the platelets were varied in dependence on the sample resistance between 10^{-9} and 10^{-4} A and 0.4 and 11 Hz, respectively. The voltage drop across the potential contacts was measured using the lock-in technique. The samples were generally cooled in zero magnetic field down to the lowest temperature. The magnetoresistance was measured when the magnetic field B was dynamically swept with a rate of 1 T/min up to 4 T and back to 0 T. Then the temperature was raised and the magnetoresistance cycle was repeated.

The AC magnetic susceptibility (field amplitude 0.3 mT and frequency 900 Hz) and the static magnetization in fields up to 5 T have been measured by means of a commercial SQUID magnetometer.

Complete structural determination for samples $x = 0.0$, 0.05, 0.10, and 0.15 was achieved by the powder neutron diffraction on the diffractometer E3 ad Hahn-Meitner-Institut in Berlin. The diffraction patterns were taken at $\lambda = 2.450$ Å over a range of $2\theta = 30°$–$110°$ in step of 0.2° with the help of curved position sensitive ^{3}He multicounter. In order to investigate magnetic arrangements and their evolution, additional measurements were performed in the range of $2\theta = 15°$–$95°$ at selected temperatures down to 4 K. The structural refinement has been done by a profile analysis using the program FULLPROF. The accuracy of the lattice parameters obtained at room temperature was checked by an alternative determination by the X-ray diffraction. An excellent agreement was achieved even for samples with very small orthorhombic deformation.

RESULTS

The results of the structural determination and electric transport measurements on the nearly stoichiometric samples $Pr_{1-x}K_xMnO_3$ with $x = 0$, 0.05, 0.10, and 0.15 are summarized in Tables 1–4. These samples are complemented

TABLE 1
Chemical and Valence Composition and the Electric Transport Properties of the $Pr_{1-x}K_xMnO_3$ Samples

x	Composition[a]	S_{290} [μVK^{-1}]	ρ_{290} (Ωm)	ε_{290} (eV)
0.00	$Pr^{3+}_{0.99}Mn^{3+}_{0.95}Mn^{4+}_{0.04}O_3$	400	2.45	0.21
0.05	$Pr^{3+}_{0.95(2)}K^{+}_{0.05(1)}Mn^{3+}_{0.895(10)}Mn^{4+}_{0.105}O_{3.00}$	240	0.113	0.17
0.10	$Pr^{3+}_{0.90(2)}K^{+}_{0.10(1)}Mn^{3+}_{0.79(1)}Mn^{4+}_{0.21}O_{3.00}$	59	0.0049	0.15
0.15	$Pr^{3+}_{0.87(2)}K^{+}_{0.14(2)}Mn^{3+}_{0.70(1)}Mn^{4+}_{0.29}O_{3.00}$	15	0.0015	0.14
0.05*n*	$Pr^{3+}_{0.93}K^{+}_{0.05}Mn^{3+}_{0.79}Mn^{4+}_{0.20}O_3$	72	—	—
0.15*n*	$Pr^{3+}_{0.85}K^{+}_{0.15}Mn^{3+}_{0.80}Mn^{4+}_{0.20}O_{2.95}$	47	—	—

[a]Mn^{4+} content determined by the idometric titration; cation compositions and their variations (in parentheses) by the electron microprobe

with two nonstoichiometric (furnace cooled) samples denoted as $x = 0.05n$ and $0.15n$.

The data in Table 1 give the Mn^{4+} content determined by the chemical analysis and the room temperature values of thermopower, electrical resistivity, and its activation. The actual compositions for samples $x = 0$ and $0.05n$ were reformulated in order to account for the expected cation deficiency in specimens with Mn^{4+} excess. We note that the presence of both cation vacancies was experimentally proved by the neutron diffraction (9) and by the high-resolution electron microscopy (10) in perovskites $LaMnO_3$ which were prepared under oxidizing conditions. For other studied samples $x = 0.05$, 0.10, and 0.15, the compositions given in Table 1 are based on the electron microprobe analysis. It is seen that the overall cation stoichiometry agrees with the nominal compositions. Moreover, the profile analysis over different spots of the ceramics revealed good spatial cationic homogeneity.

The lattice parameters at 290 and 4 K found by the neutron diffraction are listed in Table 2. The results show that the cell dimensions depend more critically on the manganese valence than on the extent of potassium substitution. To demonstrate this effect, the unit cell volume and the extent of the orthorhombic deformation of $Pr_{1-x}K_xMnO_3$ in dependence on the actual Mn^{4+} content are shown in Fig. 1.

TABLE 2
Lattice Parameters and the Unit Cell Volume in $Pr_{1-x}K_xMnO_3$

x	T (K)	a (Å)	b (Å)	c (Å)	V (Å^3)
0.00	290	5.450(1)	5.786(1)	7.589(2)	239.31
	4	5.445(2)	5.774(2)	7.554(2)	237.49
0.05	290	5.462(1)	5.677(1)	7.633(2)	236.68
	4	5.448(2)	5.676(2)	7.579(2)	234.36
0.10	290	5.478(1)	5.504(1)	7.735(2)	233.22
	4	5.464(2)	5.492(2)	7.708(3)	231.30
0.15	290	5.459(2)	5.481(2)	7.714(2)	230.81
	4	5.450(2)	5.473(2)	7.692(3)	229.44
0.05*n*[a]	290	5.472(2)	5.524(2)	7.708(2)	232.99
	4	5.462(2)	5.520(2)	7.686(3)	231.73
0.15*n*[a]	290	5.474(2)	5.493(2)	7.733(3)	232.52

[a]Nonstoichiometric samples.

The structural determination of $Pr_{1-x}K_xMnO_3$ has been performed in the space group *Pbnm*. The refinement of the potassium population in the praseodymium sites was attempted for samples with maximum substitution, $x = 0.15$ and $0.15n$, supposing full occupation of large-cation sites in these specimens. The results agreed with the nominal composition within the experimental uncertainty of $\Delta x = 0.03$. Similar agreement has been achieved by analysis of the X-ray diffraction patterns.

The atomic coordinates within the space group *Pbnm* are summarized in Table 3. The displayed data refer to the room temperature. No significant changes toward the low temperatures were observed, however. Because of limited 2θ range of the neutron diffraction patterns, the data appeared insensitive to the temperature factors. Therefore, the fixed values of $B = 0.5$ Å^2 for cations and 1.0 Å^2 for oxygen atoms were used at the refinement. The poorer fit of the observed and calculated profiles, expressed by the reliability factors R_{wp} in Table 3, was influenced mainly by the use and performance of the position sensitive multicounter.

The data on the magnetic ordering directly observed by the neutron diffraction are summarized in Table 4. As an example of a canted magnetic arrangement, the diffraction pattern for sample $x = 0.05$ is shown in Fig. 2. The antiferromagnetic component of ordered spins is evidenced by lines $h + k = 2n$, $l = 2n + 1$, whereas the ferromagnetic component contributes to lines $h + k = 2n$, $l = 2$n. The ordering temperature T_N and T_C have been determined generally from the temperature evolution of the strongest magnetic lines 001 and 110 + 002, respectively. The values obtained are compared in Table 4 with similar data derived from the AC susceptibility measurements. For $x = 0$ and 0.05 the magnetic transition temperatures correspond to the position of a sharp peak of the magnetic susceptibility in

TABLE 3
Neutron Diffraction Data for $Pr_{1-x}K_xMnO_3$ (Atomic Coordinates, Selected Distances, and Angles, Space Group *Pbnm*)

x	0.0[a]	0.0	0.05	0.05*n*[b]	0.10	0.15*n*[b]	0.15
Mn							
x	0.500	0.500	0.500	0.500	0.500	0.500	0.500
y	0	0	0	0	0	0	0
z	0	0	0	0	0	0	0
Pr, K							
x	0.008	−0.017(3)	−0.016(4)	−0.007(5)	−0.004(8)	0.011(5)	0.015(8)
y	0.064	0.066(2)	0.063(3)	0.037(2)	0.044(3)	0.038(3)	0.030(4)
z	0.250	0.250	0.250	0.250	0.250	0.250	0.250
OI							
x	0.075	0.084(2)	0.078(2)	0.074(2)	0.076(3)	0.062(4)	0.075(4)
y	0.476	0.484(2)	0.488(2)	0.487(2)	0.491(3)	0.493(3)	0.496(5)
z	0.250	0.250	0.250	0.250	0.250	0.250	0.250
OII							
x	−0.295	−0.284(2)	−0.284(2)	−0.280(2)	−0.283(2)	−0.286(2)	−0.275(3)
y	0.314	0.313(1)	0.304(1)	0.291(1)	0.283(2)	0.284(2)	0.279(3)
z	0.046	0.042(1)	0.036(1)	0.039(1)	0.033(1)	0.037(2)	0.030(2)
R_{wp}		*6.86*	*9.04*		*7.64*		*9.50*
R_{exp}		*2.27*	*1.96*		*2.02*		*1.93*
R_B		*5.55*	*3.27*		*3.19*		*4.15*
Mn–OI	1.94	1.96(1)	1.95(1)	1.97(1)	1.98(2)	1.96(1)	1.97(2)
Mn–OII	2.16	2.19(1)	2.12(1)	2.03(1)	1.99(2)	1.99(1)	1.97(2)
Mn–OII	1.96	1.92(1)	1.94(1)	1.94(1)	1.97(2)	1.97(1)	1.95(2)
Mn–OI–Mn	154	152(1)	154(1)	156(1)	156(1)	160(1)	156(1)
Mn–OII–Mn	149	152(1)	155(1)	156(1)	158(1)	157(1)	161(1)

[a]Ref. (12), $a = 5.445$ Å, $b = 5.787$ Å, $c = 7.575$ Å.
[b]Nonstoichiometric samples, investigated at a different facility.

Fig. 3, whereas for ferromagnetic samples $x = 0.10$ and 0.15 the T_C values were obtained by analyzing the Curie–Weiss behavior of susceptibility above the ordering temperature.

The temperature dependence of the electrical resistivity registered in zero magnetic field is shown in Fig. 4. The activation energy for the conduction mechanism in the paramagnetic region is nearly temperature independent for all samples and slowly decreased from $\varepsilon = 0.21$ eV for $x = 0$ to 0.14 eV for $x = 0.15$ (See also Table 1). Both purely ferromagnetic samples $x = 0.10$ and 0.15 show an anomaly at T_C (126 and 134 K, respectively) which can be interpreted as a lowering of the activation energy below T_C.

The ferromagnetic transitions are further evidenced by the temperature dependence of thermopower shown in

TABLE 4
Magnetic Arrangements, Critical Temperatures, and the Ordered Moments (in Bohr Magnetons) for $Pr_{1-x}K_xMnO_3$

x	$\%Mn^{4+}$	Type	T_N	T_C	$T_{N,C}$[a]	m_{AF}(Mn)	m_F(Mn)	m_F(Pr)[b]	m_F(Mn + Pr)[c]
0.00	4	AF	95		94	3.54(10)	0.0(2)	—	—
0.05	10.5	Canted	85	85	86	2.64(8)	1.05(20)	0.12(20)	0.90
0.10	21	F		125	126		3.71(12)	0.37(11)	3.76
0.15	29	F		130	134		3.42(14)	0.38(11)	3.76
0.05*n*	20	F		85	—		3.1(1)	0.4	—
0.15*n*	20	F		120	—		3.7(1)	0.4	—

[a]Critical temperatures deduced from the AC susceptibility data in Fig. 3.
[b]Mean moment per one Pr, K site.
[c]Ferromagnetic moment per formula unit by the magnetization measurements.

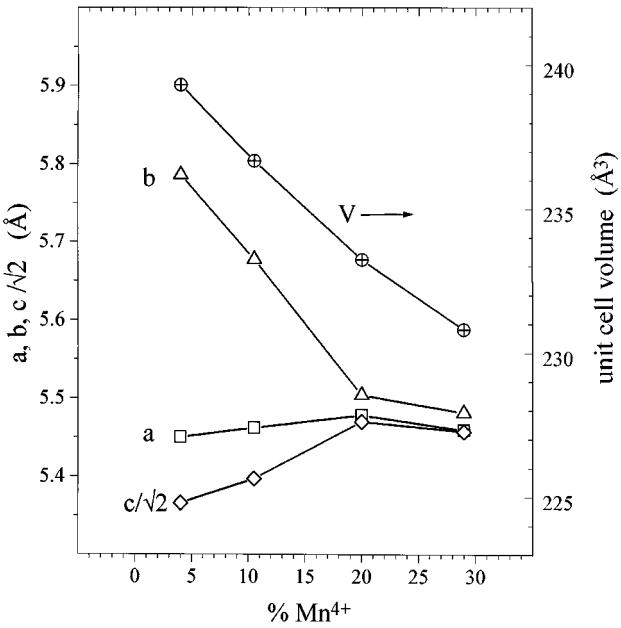

FIG. 1. Lattice parameters and the unit cell volume in $Pr_{1-x}K_xMnO_3$ ($x = 0$, 0.05, 0.10, and 0.15) vs the actual Mn^{4+} content.

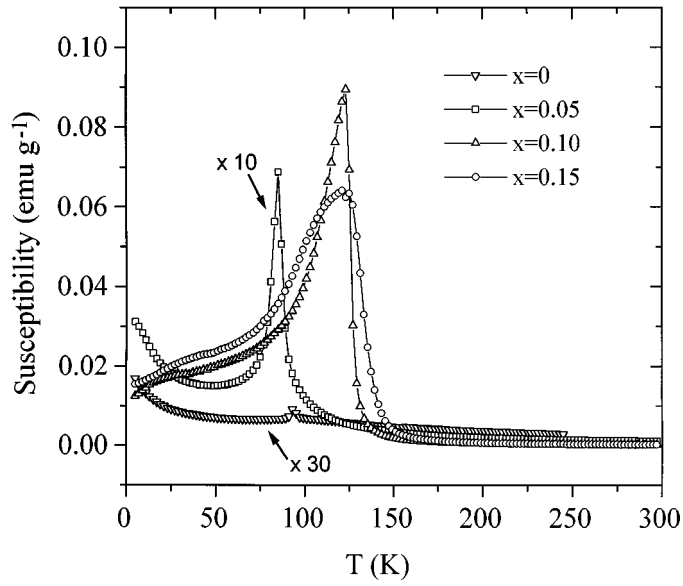

FIG. 3. AC susceptibility in $Pr_{1-x}K_xMnO_3$.

Fig. 5. It is seen that the positive thermopower starts to fall down below T_C. An interesting feature is encountered for $x = 0.15$ where the thermopower becomes negative below ~ 100 K; then it achieves a broad minimum of $-20\ \mu V K^{-1}$ at ~ 60 K and returns thermodynamically to zero at 0 K. Other samples, the antiferromagnetic $x = 0$ ($T_N = 94$ K) and canted $x = 0.05$ ($T_C = T_N = 86$ K) exhibit high and positive thermopower which increases monotonously with decreasing temperature. Observed behavior is typical for systems with thermal activation of hole-like carriers with characteristic energies of $\varepsilon_a = 0.06$ and 0.04 eV for $x = 0$ and $x = 0.05$, respectively.

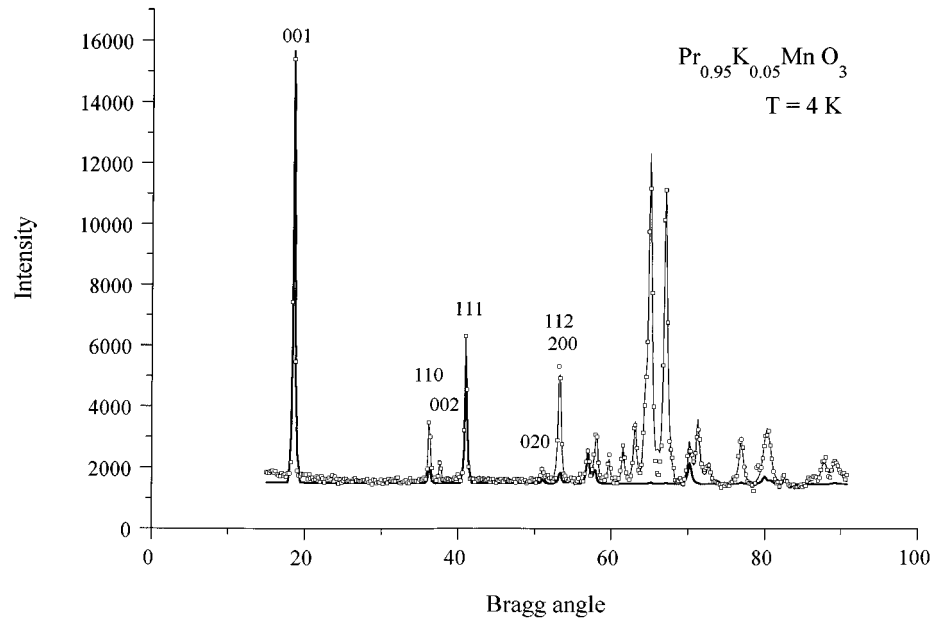

FIG. 2. Neutron diffraction pattern of $Pr_{0.95}K_{0.05}MnO_3$ at 4 K (The observed and calculated profiles are shown by the open symbols and the thin line, respectively; the magnetic contribution is marked by the heavy line.)

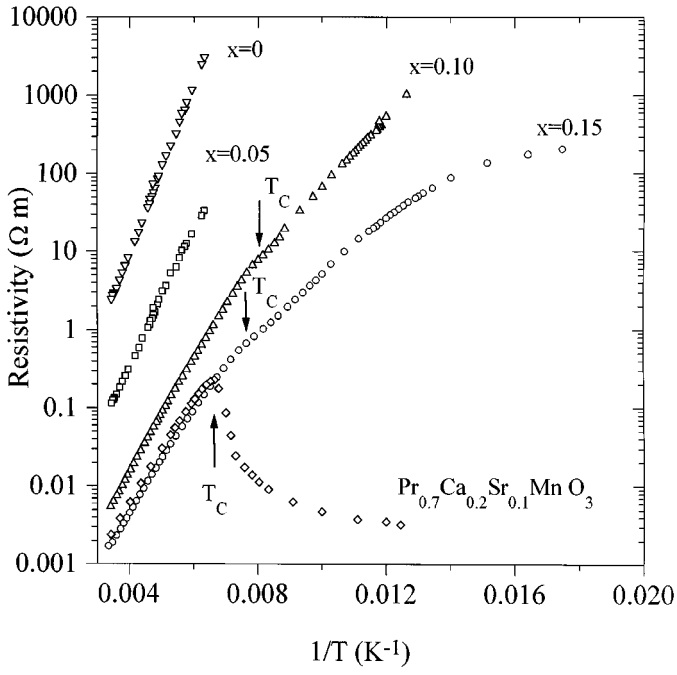

FIG. 4. Resistivity in $Pr_{1-x}K_xMnO_3$ (the arrows mark the ferromagnetic transitions; sample $x = 0.15$ is compared with $Pr_{0.07}Ca_{0.2}Sr_{0.1}MnO_3$ (Ref. 8)).

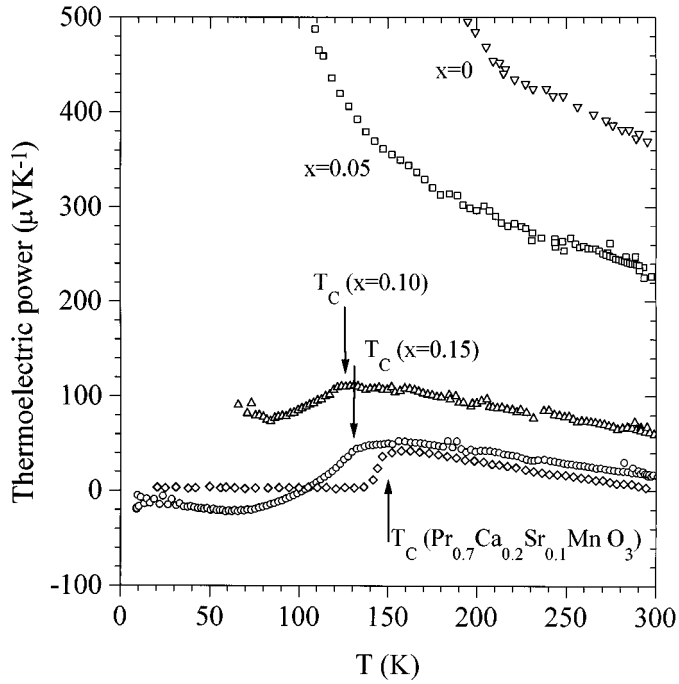

FIG. 5. The thermoelectric power in $Pr_{1-x}K_xMnO_3$ (the arrows mark the ferromagnetic transitions; sample $x = 0.15$ is compared with $Pr_{0.7}Ca_{0.2}Sr_{0.1}MnO_3$ (Ref. 14)).

Measurements of the magnetoresistance have been performed on the ferromagnetic samples for selected temperatures. The results in the logarithmic scale are displayed in Fig. 6. It is clearly evidenced that in weak magnetic fields the maximum negative magnetoresistance is achieved very close to T_C. For $x = 0.15$ the field dependences in Fig. 6 and the temperature scans in Fig. 7 show, however, that the situation is changed in higher fields. The negative magnetoresistance experiences at T_C only a local maximum; then it increases further with decreasing temperature. Moreover, the $\ln(R)$ vs B dependence becomes linear for temperatures below 90 K and fields above 0.5 T so that an appreciable magnetoresistance remains practically constant over a range of magnetic fields where the magnetization is already saturated (see the magnetization curves in Fig. 8). Let us note that the relative change of resistivity makes about 40% per one Tesla at the lowest investigated temperature of 50 K.

DISCUSSION

The electron microprobe analysis and the neutron diffraction experiments on $Pr_{1-x}K_xMnO_3$ show that potassium enters the perovskite structure and is substitutional for praseodymium. The maximum solubility is estimated to $x = 0.175$. In contrast with the systems $Pr_{1-x}A_x^{2+}MnO_3$ (A = Ca, Sr, Ba) where the actual Mn^{4+} content seems to be controlled mostly by the extent of the divalent substitution, the sintering temperature, atmosphere, and, of course, the cooling conditions appeared critical in the case of K^+ substitution. This was demonstrated by the same Mn^{4+} content of 20% achieved in the furnace-cooled samples with nominal potassium concentration ranging from 0.05 up to 0.15 (See Table 1). The state of these samples is a compromise between decreasing oxygen diffusion and increasing oxygen activity at the cooling and, as we have found, corresponds to an equilibrium at about 900°C. To achieve stoichiometric samples throughout the whole $Pr_{1-x}K_x$ MnO_3 system it is, therefore, necessary either to vary the annealing temperatures (in air 1300–1400°C for $x = 0$ and assumedly 700°C for $x = 0.15$) or to vary partial oxygen pressure to above seven orders of magnitude at a constant temperature.

All studied samples belong to orthoperovskites of the *Pbnm* symmetry which are characterized by certain kind of cooperative tilting of MnO_6 octahedra (so-called buckling). The macroscopic orthorhombic deformation which originates from the buckling is further increased enormously by the cooperative Jahn–Teller (JT) ordering (see, e.g., Ref. 11) in samples with high Mn^{3+} content. The dependence of the lattice parameters shown in Fig. 1 suggests that the concentration boundary between the JT-ordered and JT-disordered structures occurs at about 20% of Mn^{4+}.

The Jahn–Teller ordering is manifested essentially by distortion of the MnO_6 octahedra. The calculation of

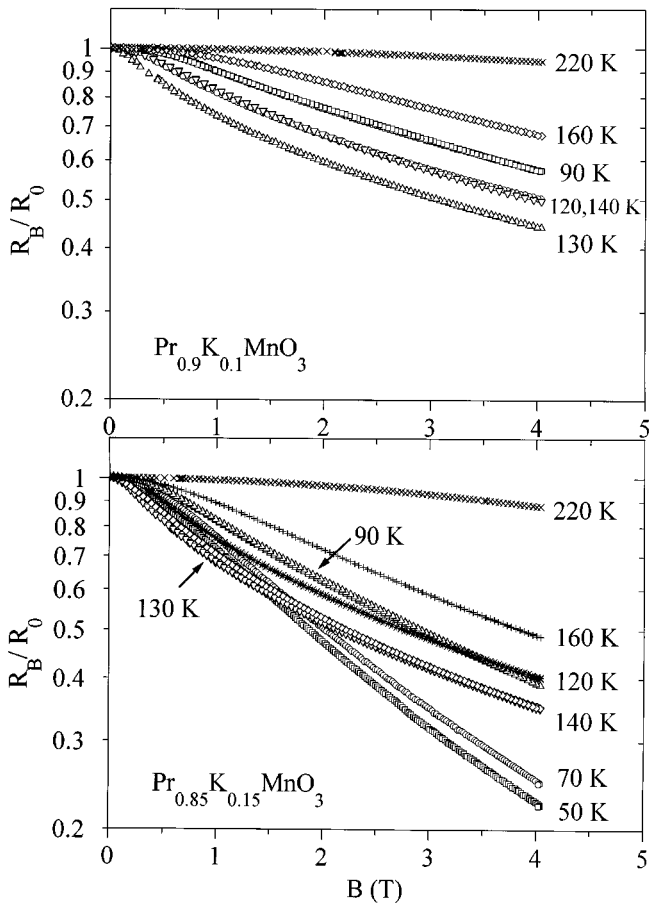

FIG. 6. The magnetoresistance at selected temperatures for ferromagnets $Pr_{0.9}K_{0.1}MnO_3$ ($T_C = 126$ K) and $Pr_{0.85}K_{0.15}MnO_3$ ($T_C = 134$ K).

interatomic distances and angles showed for all samples that the the octahedron axes were mutually perpendicular within the experimental uncertainty of about 1°. The observed Mn–O distances in Table 3 clearly show a distortion of the octahedron for JT-ordered samples $x = 0$ and 0.05, which consists of considerable tetragonal elongation with some admixture of an orthorhombic component. The MnO_6 octahedra for other samples $x = 0.10$ and 0.15 are practically regular. The tilting of the octahedra which is characterized by the Mn–O–Mn angles (also included in Table 3) is nearly constant throughout the series.

The magnetic structures in the $Pr_{1-x}K_xMnO_3$ series, which are summarized in Table 4, reflect a competition of two main magnetic interactions—the Mn–O–Mn superexchange and the double exchange. According to Goodenough–Kanamori rules, the superexchange interactions in $PrMnO_3$ are ferromagnetic within the (001) layers and antiferromagnetic between these layers. Such layered antiferromagnetism is in fact observed in our sample $x = 0$ with actual Mn^{4+} content of 4%. The manganese moments are aligned along the *b*-direction. Their ordered magnitude amounts to 3.54 μ_B and observed Neel temperature is 94 K. These data agree very well with an early neutron diffraction investigation on $PrMnO_3$ by Quezel-Ambrunaz (12). The discrepancy between the observed magnetic moment and the theoretical value for Mn^{3+} of 4 μ_B may arise due to possible local defects associated with excessive Mn^{4+} ions in the samples.

With increasing Mn^{4+} content a canting arises between successive (001) ferromagnetic layers. This is due to the double exchange mechanism which is mediated by itinerant carriers originating from disordered Mn^{3+} and Mn^4 pairs. Such long-range ordered canted structure is formed at low temperatures for sample $x = 0.05$ (10.5% Mn^{4+}) as was demonstrated in Fig. 2. In this sample the manganese moments possess an antiferromagentic component of 2.64 μ_B along the *b*-direction and a ferromagnetic component of 1.05 μ_B along the *c*-direction, making a canting angle of about 140°. We note that the antiferromagnetic and ferromagnetic components displayed similar temperature dependences and, consequently, the Néel and Curie temperatures coincide ($T = 86$ K). This seems to be a general behavior of the canted structures (13).

The samples $x = 0.10$ and 0.15 exhibit purely ferromagnetic phases. The observed manganese moments of 3.71 and 3.42 μ_B (Table 4) are slightly lower than the theoretical values 3.8 and 3.7 μ_B, respectively. In addition, small ordered moments of about 0.4 μ_B per Pr^{3+} ion, induced by the ferromagnetically aligned manganese spins, are observed at the rare earth sites. The sum of the manganese and praseodymium ferromagnetic moments is in reasonable agreement with measurements of spontaneous magnetization.

The electric conductivity in the $Pr_{1-x}K_xMnO_3$ series remains thermally activated even at the maximum potassium content. Except for some anomaly at T_C there is no sign of the I–M transition which is frequent for analogous ferromagnetic systems. Instead, the resistivity for $x = 0.15$ is apparently saturated at low temperatures on a high value of 200 Ωm. Such behavior is in a striking variance with the simultaneous ferromagnetic and I–M transition observed earlier on a related perovskite $Pr_{0.7}Ca_{0.2}Sr_{0.1}MnO_3$ which exhibited otherwise similar room temperature resistance, Curie temperature T_C, and the Mn^{4+} content (8). The I–M transition in this compound is also demonstrated in Fig. 4 by the step-like drop of the thermopower to nearly zero (metallic) value just at T_C (14). We relate the different properties of $Pr_{0.85}K_{0.15}MnO_3$ to a discrepancy of the Pr^{3+} and K^+ valencies and, especially, to a large variance of ionic radii ($r_{Pr}(IX) = 1.18$, $r_K(IX) = 1.55$). It should be noted in this context that the observed $T_C = 134$ K is about to 200 K lower than one would expect from the mean large-cation size, taking into account the general diagram for systems with 30% of Mn^{4+} (15). The role of dissimilar substituent seems to apply also for $Pr_{0.7}Ba_{0.3}MnO_3$ ($r_{Ba}(IX) = 1.47$) for which a rather low $T_C = 195$ K and diffusive I–M transition

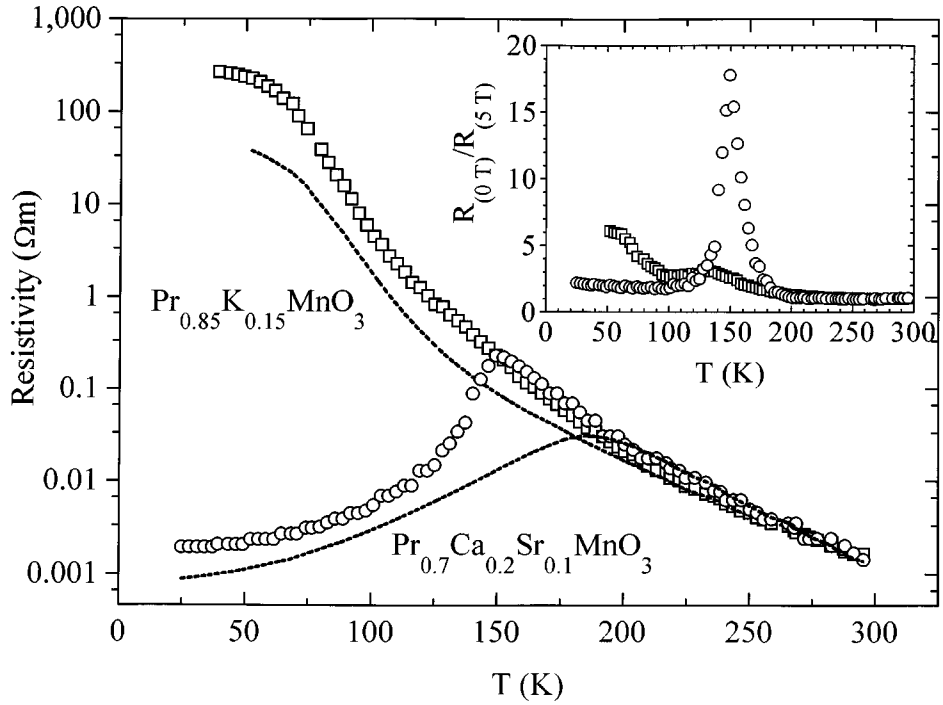

FIG. 7 Temperature dependence of resistivity for $Pr_{0.85}K_{0.15}MnO_3$ and $Pr_{0.7}Ca_{0.2}Sr_{0.1}MnO_3$ measured in $B = 0$ (symbols) and 5 T (dashed lines).

were reported (6). On the other hand, we have observed that the praseodymium and lanthanum systems with monovalent substitution by smaller natrium ($r_{Na}(IX) = 1.24$) could fit the phase diagram in Ref. (15) fairly well.

In summary, we have prepared perovskites $Pr_{1-x}K_xMnO_3$ up to the maximum content of 30% Mn^{4+}, which corresponded to the ideal sample of $x = 0.15$. As to the crystal structure and magnetic ordering, the potassium

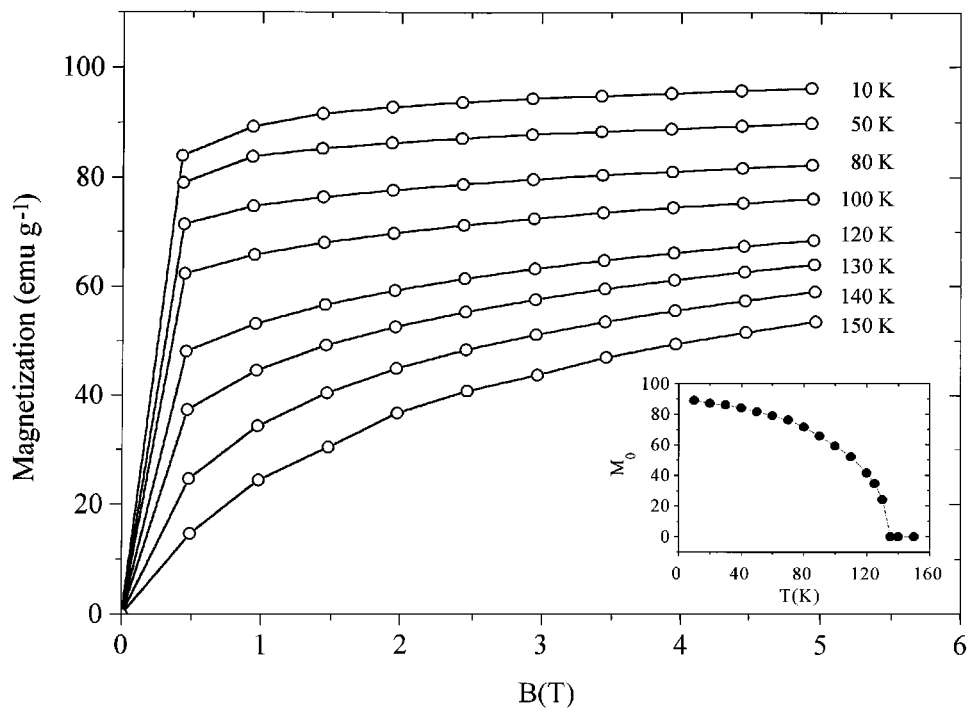

FIG. 8 Magnetization curves for $Pr_{0.85}K_{0.15}MnO_3$ (the inset shows spontaneous moment vs temperature derived from Arrot plots).

system behaves similarly to manganites with divalent substitutions (Ca, Sr, Ba) and the same Mn^{4+} content. In particular, the concentration transition from the antiferromagnetic ordering for $PrMnO_3$ to the ferromagnetic one for 20% of Mn^{4+} ($x = 0.10$ for the potassium system) involves true canted arrangements. This supports the conception of the double exchange interactions between the disordered Mn^{3+}, Mn^{4+} pairs and suggests that the charge carriers generated by the monovalent substitution should be itinerant. The electrical conduction is, however, thermally activated even for maximum doping and temperatures well below the ferromagnetic transition. The lack of the I–M transition and other characteristics of the $Pr_{0.85}K_{0.15}MnO_3$ sample, which are in variance with previously studied manganites with 30% of Mn^{4+}, reflect the large size mismatch of Pr and K ions. A more complex comparison of these systems, including data on the specific heat and thermal conductivity, will be published elsewhere (16).

ACKNOWLEDGMENTS

The research was performed under a support of the Grant Agency of the Czech Republic (Grant 202/94/0065). Experiments at Hahn-Meitner-Institut in Berlin were supported by the European Commission through the Human Capital and Mobility (PECO) programme "Access to large-scale facilities." One part of the work was carried out under the financial support of the Belgian Office for Scientific, Technical and Cultural Affairs in Louvain-la-Neuve, Unité de Physico-Chemie et de Physique des Matriaux, UGL, Belgium. J.H. acknowledges this support and thanks J.P. Issi, E. Griveri, and S. Dubois for helpful discussions. The authors are greatly indebted to D. Zemanová for the chemical analyses.

REFERENCES

1. S. Jin, T. H. Tiefel, M. McCormack, R. A. Fastnacht, R. Ramesh, and L. H. Chen, *Science* **264,** 413 (1994).
2. C. N. R. Rao and A. K. Cheetham, *Science* **272,** 5260 (1996).
3. Y. Tokura, Y. Tomioka, H. Kuwahara, A. Asamitsu, Y. Morimoto, and M. Kasai, *J. Appl. Phys.* **79,** 5288 (1996).
4. Z. Jirák, S. Krupička, Z. Šimša, M. Dlouhá, and S. Vratislav, *J. Magn. Magn. Mater.* **53,** 153 (1985).
5. K. Knížek, Z. Jirák, E. Pollert, F. Zounová, and S. Vratislav, *J. Solid State Chem.* **100,** 192 (1992).
6. Z. Jirák, E. Pollert, A. F. Andresen, J-C. Grenier, and P. Hagenmuller, *Eur. J. Solid State Inorg. Chem.* **27,** 421 (1990).
7. Y. Tomioka, A. Akamitsu, Y. Morimoto, and Y. Tokura, *J. Phys. Soc. Jpn.* **64,** 3626 (1995); H. Yoshizawa, H. Kawano, Y. Tomioka, and Y. Tokura, *Phys. Rev. B* **52,** R13145 (1995).
8. B. Raveau, A. Maignan, and V. Caignaert, *J. Solid State Chem.* **117,** 424 (1995).
9. J. A. M. van Roosmalen, E. H. P. Cordfunke, R. B. Helmholdt, and H. W. Zandbergen, *J. Solid State Chem.* **110,** 100 (1994).
10. H. Cerva, *J. Solid State Chem.* **120,** 175 (1995).
11. Z. Jirák, *Phys. Rev. B* **46,** 8725 (1992).
12. S. Quezel-Ambrunaz, *Bull. Soc. Fr. Minér. Crist.* **91,** 339 (1968).
13. Z. Jirak *et al.*, *J. Appl. Phys.* **81,** 5790 (1997).
14. J. Hejtmánek, Z. Jirák, D. Sedmidubský, A. Maignan, Ch. Simon, V. Caignaert, C. Martin, and B. Raveau, *Phys. Rev. B* **54,** 11947 (1996).
15. H. Y. Hwang, S.-W. Cheong, R. G. Radaelli, M. Marezio, and B. Batlogg, *Phys. Rev. Lett.* **75,** 914 (1995).
16. J. Hejtmánek *et al.*, *J. Appl. Phys.* **81,** 4975 (1997).